Rb-Sr isotopic characterization of pegmatite dikes from the Tuolumne Intrusive Suite, California, USA

Christopher J. Doorn[1]

[1]*University of North Carolina at Chapel Hill, Department of Geological Sciences*

ABSTRACT

Pegmatite dikes are common in granitic plutons and reflect crystallization of the fluid-rich last increments of the system. I measured $^{87}Sr/^{86}Sr$ ratios for several pegmatites from the Tuolumne Intrusive Suite in the Sierra Nevada batholith, California to examine the possible role of mass transfer between wall rocks and intruding magma. Variation in isotopic composition between wall rocks and plutons provides a sensitive test of fluid-rock interaction.

Meter-scale pegmatite dikes along the margins of the intrusive suite cut both wall rocks and granitoids (including tonalite, granodiorite, and granite). Initial $^{87}Sr/^{86}Sr$ ratios in granitoids along an east-west traverse range from 0.7057 to 0.7066 (Kistler et al, 1986; Bateman et al., 1988; Gray et al., 2008). Wall rocks along the margins of the suite display variable $^{87}Sr/^{86}Sr$, ranging from 0.710 to 0.774 (Mills et al., 2009), significantly more radiogenic than the igneous materials. Age-corrected pegmatite $^{87}Sr/^{86}Sr$ ratios range from 0.706 to 0.709.

Pegmatites have higher $^{87}Sr/^{86}Sr$ ratios than granitoids, but lower than the metasedimentary wall rocks. I interpret these data as indicating interaction between hydrous fluids from late-stage granite crystallization and wall rocks. Pegmatites in the Tuolumne Intrusive Suite represent the final stages of pluton development, and hydrothermal circulation could drive fluid paths that traverse wall rocks and the crystallizing plutons, resulting in $^{87}Sr/^{86}Sr$ ratios between those of the two end members.

INTRODUCTION

Interaction between intruding magma and surrounding wall rock is broadly assumed, but geochemical data for this interaction are difficult to obtain. However, pegmatites may record mass exchange between intruding magmas and wall rocks. Although most studies of pegmatites concern their classification and mineralogy, pegmatites also represent the final stages of crystallization of plutonic systems. Processes governing pegmatite growth are still poorly understood.

A comparison of initial $^{87}Sr/^{86}Sr$ ratios across lithologies may indicate whether pegmatites record mass exchange; initial $^{87}Sr/^{86}Sr$ is a robust indicator of interaction because these isotopes do not fractionate during crystallization. Initial $^{87}Sr/^{86}Sr$ ratios are far greater in wall rocks than in adjacent plutonic rocks (Kistler et al., 1986; Bateman et al., 1988; Gray et al., 2008; Mills et al., 2009; Gross, 2015). I sampled pegmatites at four locations throughout the Tuolumne Intrusive Suite in the Sierra Nevada batholith and calculated their initial $^{87}Sr/^{86}Sr$ ratios. If the pegmatites record interaction between magma-derived hydrothermal fluids and wall rock, their isotopic ratios should be intermediate between the groups.

Pegmatite Petrogenesis

Jahns and Burnham (1969) described mechanisms for producing pegmatite from cooling granitic magma. As magma crystallizes anhydrous phases, the remaining liquid becomes enriched in water. Once the melt phase becomes water-saturated, fluid exsolves as a new phase, and pegmatites crystallize rapidly at low temperatures from such hydrothermal phases (Jahns and Burnham, 1969). This fractionation model for producing pegmatite was supported by Roda-Robles (2012) and Ballouard et al. (2015), which argued that pegmatites were derived from host granitoids by fractional crystallization.

Water reduces magma viscosity, nucleation rate, and polymerization, while increasing diffusivity and the ability for a melt to dissolve surrounding material (Simmons and Webber, 2007; Nabelek et al., 2010). Less viscous magma can more easily propagate as dikes, and increased capacity for magmas to dissolve may enable interaction with intruded materials. Elevated diffusivity and lower nucleation rates promote crystal growth, generating coarse textures characteristic of pegmatite (Jahns and Burnham, 1969, Davidson and Thomas, 2012).

Kontak et al. (2002) noted that devolatization of metasedimentary xenoliths may be a potential source of water for hydrothermal fluids. However, simultaneous release of CO_2 would reduce the activity of water and offset a metasedimentary water contribution. A granitic magma containing a few percent water by mass should concentrate enough water in the remaining melt during crystallization to exsolve a fluid phase by later stages of cooling.

Ballouard et al. (2015) argued that the Hercynian Guérande leucogranite of the Armorican Massif in France underwent alteration by hydrothermal fluids exsolved during cooling. Multiple pegmatite dikes and quartz veins through the leucogranite are thought to have crystallized from hydrothermal fluids. Therefore, Ballouard et al. (2015) concluded that fluids which caused hydrothermal alteration were involved in crystallizing pegmatites in the same plutonic body. Pegmatites have been documented as records of agents of hydrothermal alteration.

GEOLOGIC SETTING

The Sierra Nevada batholith (SNB) in eastern California (Fig. 1) makes up much of the Sierra Nevada range and spans about 600 km, trending NNW. The width of the batholith averages 100 to 120 km. The SNB lies between the Basin and Range to the east and the Great Valley to the west; the south end of the SNB is separated from the Mojave Desert by the Garlock fault, and the north end abuts the Cascade Range. Emplacement ages in the SNB are younger

from west to east, with Late Cretaceous intrusive bodies forming the east-central region. The Tuolumne Intrusive Suite (TIS) of Yosemite National Park, California, in the east-central portion of the SNB, is composed of several nested plutons.

The TIS is divided into several units based on composition and texture. The oldest, exterior units of the TIS are contemporaneous granodiorites and tonalites of Glen Aulin (Kga) and Kuna Crest (Kkc) on the west and east, respectively. Inward are the equigranular (Khde) and porphyritic (Khdp) Half Dome Granodiorite, Cathedral Peak Granodiorite (Kcp), and the Johnson Granite Porphyry (Kjp). Moving from margin to core, rocks are generally more felsic with coarser, porphyritic textures, with the exception of Kjp. Hornblende, biotite, and titanite phenocrysts are abundant in Khd, and megacrystic K-feldspar is present in Kcp. Tabular rafts of megacrystic K-feldspar are present in Kcp. Contacts between these units are generally gradational (Bateman and Chappell, 1979).

Metamorphic wall rocks along the margins of the TIS include metasedimentary and metavolcanic strata. The primary wall rocks of interest here are those near May Lake in the west and Saddlebag Lake in the East (Fig. 1). The Saddlebag Lake roof pendant consists of Devonian to Triassic metavolcanic and metasedimentary rocks (Brook, 1977; Lahren et al., 1990). Metamorphic rocks near May Lake consist of calc-silicate rocks, quartzite, pelitic quartzite, pelitic hornfels, and marble (Rose, 1957; Mills et al., 2009). Foliated metamorphic rocks at May Lake strike northeast and dip northwest.

Pegmatite dikes are widespread throughout the TIS. Pegmatites along the eastern margin near Saddlebag lake (Fig. 1) intrude both Kcp and surrounding metavolcanic rocks and strike oblique to foliation. In the west, near May Lake, thicker pegmatite dikes intrude granodiorite of Kga. Rose (1957) described pegmatites containing andalusite and corundum within the May

Lake screen. The modal assemblage of pegmatites described in Rose (1957) varies from that of the TIS pegmatites, which generally contain K-feldspar, quartz, albite, and biotite. Future work might investigate whether these dikes were chemically influenced by host metavolcanic rocks.

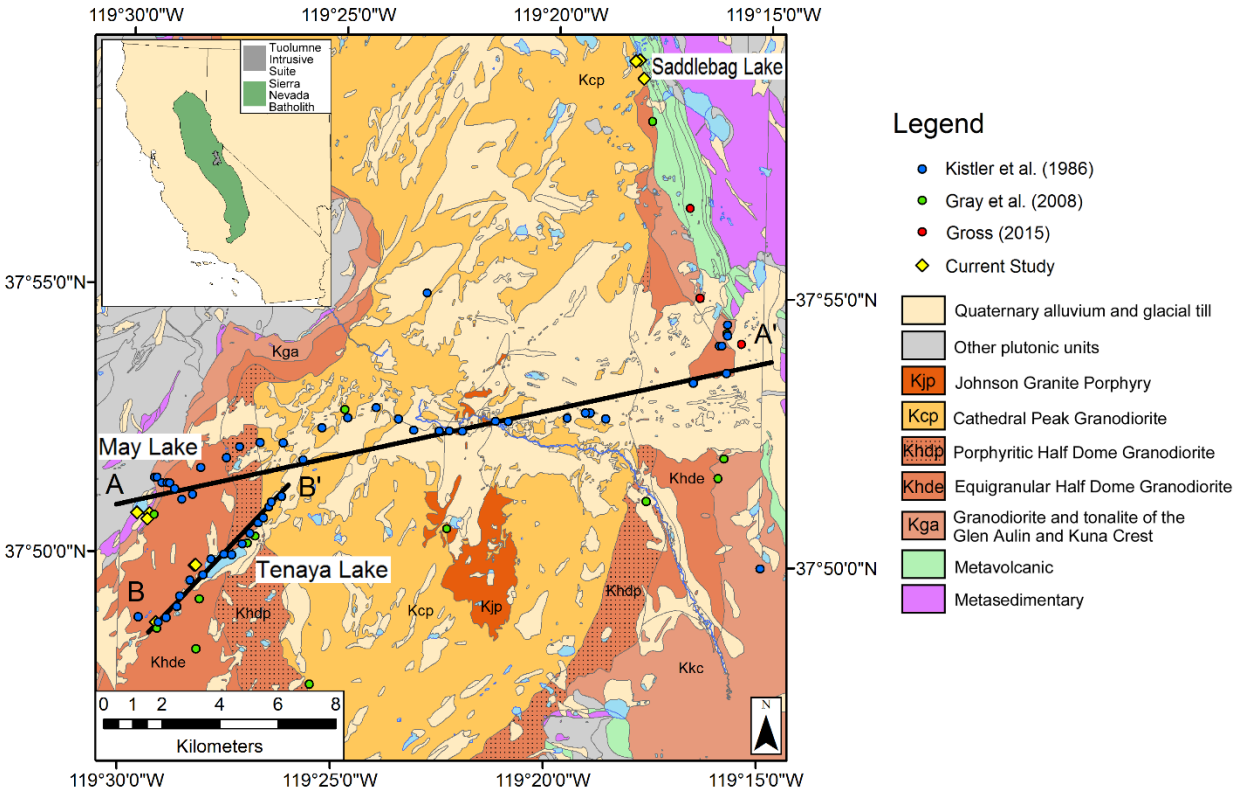

Figure 1: Geologic map of part of the Tuolumne Intrusive Suite (TIS). Unit boundaries were taken from Bateman et al. (1983). Inset shows the Sierra Nevada batholith in green with the TIS in gray.

PREVIOUS WORK

Tuolumne Intrusive Suite Rb-Sr Systematics

The TIS has long been seen as an archetype of a nested plutonic complex. Bateman and Chappell (1979) proposed that it was constructed of four separate intrusions (from oldest to youngest, Kga-Kkc, Khd, Khdp, and Kcp), each of which shouldered earlier pulses aside to form a nested, inward-younging complex. Frey et al. (1978) and Bateman and Chappell (1979)

proposed that compositional variation was controlled by crystal fractionation. However, these hypotheses are inconsistent with both thermal modeling and isotopic measurements.

Thermal modeling indicated the TIS would cool faster than permitted by geochronological evidence if it existed as amalgamated magma chambers (Glazner et al., 2004). U-Pb zircon geochronology showed that the whole suite took about 10 Ma to amalgamate (Coleman and Glazner, 1997; Coleman et al., 2004). Variation of initial $^{87}Sr/^{86}Sr$ across the suite cannot be explained by simple fractionation of a few concentric magma chambers (Kistler et al., 1986; Bateman et al., 1988; Gray et al., 2008).

Kistler et al. (1986) found that initial $^{87}Sr/^{86}Sr$ increases from 0.7057 to 0.7066 from the margin to the interior (Fig. 2). Most variation of initial $^{87}Sr/^{86}Sr$ occurs in the outer units. Mixing of mantle and crustal derivatives may produce the range of initial $^{87}Sr/^{86}Sr$ consistent with measured TIS isotopic compositions (Kistler et al., 1986). Monte Carlo simulations (Gray et al., 2008) showed that a combination of partial melting of a mantle source and mixing could produce observed compositional variation.

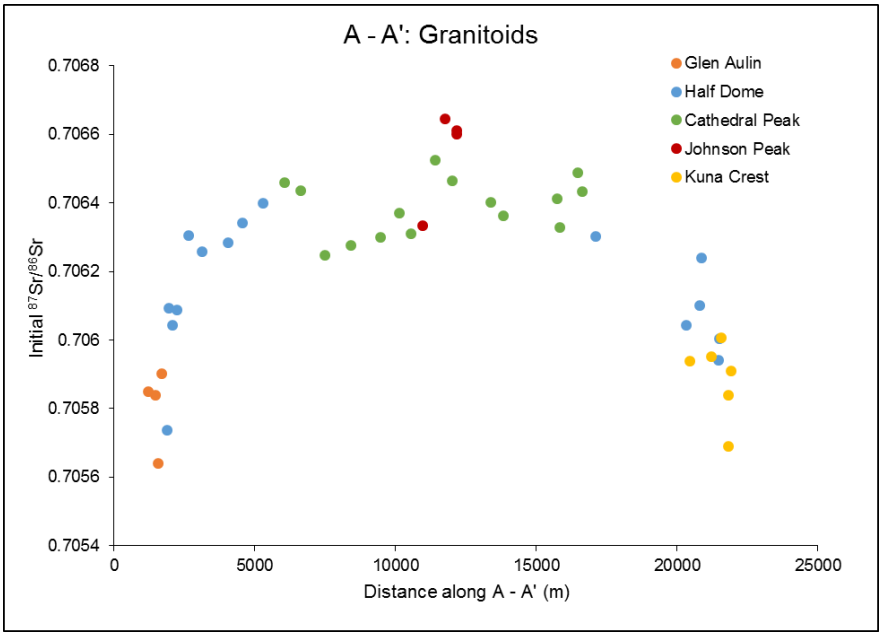

Figure 2: Initial Sr for granodiorites from Kistler et al. (1986), Bateman et al. (1988), and Gray et al. (2008). Points lie along A - A' (Fig. 1), and span the suite from the western to eastern margin. The transect starts in Kga on the west and ends in Kkc in the east.

Measured $^{87}Sr/^{86}Sr$ ratios of metasedimentary wall rocks from near May Lake age-corrected to 90 Ma ($^{87}Sr/^{86}Sr_{90}$) range from 0.710 to 0.774 (Mills et al., 2009). Mills et al. (2009) measured $^{87}Sr/^{86}Sr$ and $^{143}Nd/^{144}Nd$ in wall rocks and granitoids at May Lake to quantify interaction between the two. They found that measurable interaction was limited to within a meter or two of the contact. Spatially limited hybridization precludes geochemical influence from wall rocks on granitoids throughout the TIS. Metasedimentary rocks near Saddlebag lake have $^{87}Sr/^{86}Sr_{90}$ from 0.712 to 0.721 (Gross, 2015).

SAMPLE DESCRIPTIONS

Pegmatites, granitoids, and metasedimentary samples were collected at four locations in the TIS. Pegmatite dikes in Kga near May Lake are up to several meters thick and contain mainly K-feldspar, quartz, albite, biotite, and accessory phases including locally abundant tourmaline, Fe-Ti oxides, titanite, apatite, and zircon. K-feldspar is 10 to 20 cm along the longest axis (Fig. 3A). Quartz crystals are locally up to 3 cm in width but mostly occur as graphic intergrowths with K-feldspar and plagioclase. Zonation is not present on the outcrop scale, but some hand samples from May Lake exhibit zonation of quartz coarseness. Biotite books are about 1 x 4 cm. Books do not strike in a common orientation (Fig. 3C). Contacts are locally discolored by oxidation (Fig. 3C).

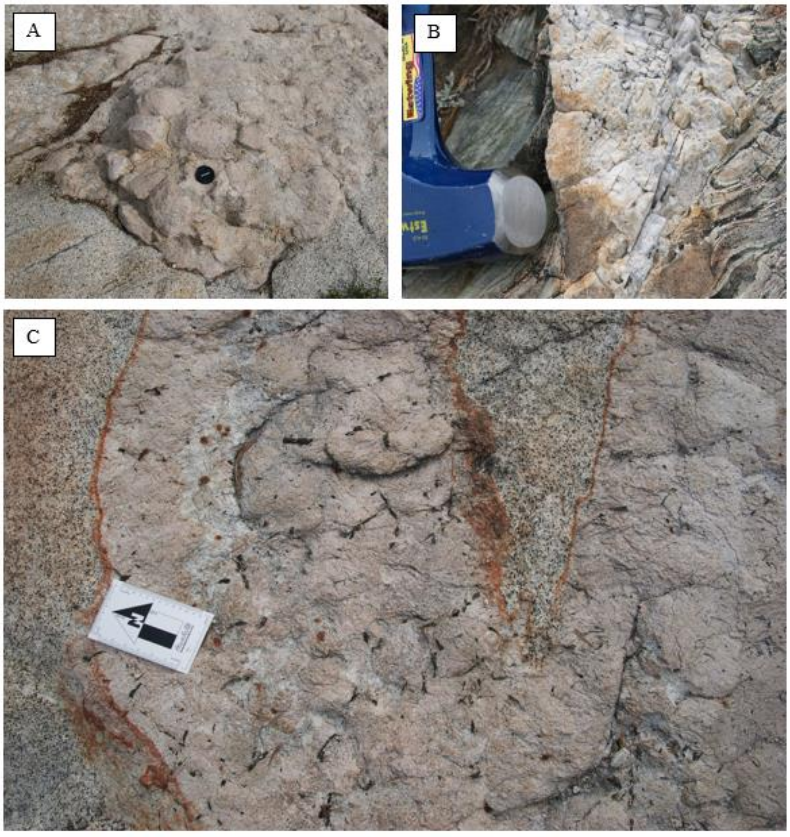

Figure 3: (a) Pegmatite outcrop east of May Lake; K -feldspar crystals are larger than 10 cm in width. The contact between pegmatite and Kga is abrupt. (b) Pegmatite dike emplaced in metavolcanic rocks near Steelhead Lake. Dikes contain mostly K-feldspar and quartz. (c) Pegmatite dikes near May Lake contain 1x4 cm biotite books oriented perpendicular to the surface.

Three samples were collected from pegmatite dikes on the eastern margin of the TIS near Saddlebag Lake. Two of these pegmatites intrude Kcp and one intrudes a metavolcanic unit. These pegmatites contain K-feldspar (2-10 cm), megacrystic quartz, and interstitial albite. Graphic quartz textures are less common than at May Lake. Perthite lamellae are visible in hand sample as parallel veins. Pegmatite dikes are oblique to foliation in wall rocks (Fig. 3B).

Additional sample areas include Kcp near Twin Lakes, Khde at Olmsted Point, and north of Tenaya Lake (Fig. 1). Pegmatites from near Olmsted Point are narrow dikes about 5 to 10 cm thick and composed of quartz and K-feldspar crystals about 1 cm across. These bodies of pegmatite are thinner than those found along the margins of the TIS. Pegmatite dikes are locally found within aplite dikes. These samples have less complex mineral assemblages than dikes along the TIS margins. Pegmatite collected from the northern portion of the Kcp, near Twin Lakes, contains mostly K-feldspar along with quartz, albite, and biotite.

METHODS

A ceramic shatterbox was used to generate fine powders suitable for dissolution and XRF analysis. Samples larger than ~ 0.6 cm were crushed in a steel jaw crusher. A steel disc mill was used to reduce samples to sand size for heavy-liquid separation. Selected K-feldspar crystals from crushing and hand samples were either mounted or made into thick sections for analysis by scanning electron microscopy.

A hand magnet was used to separate iron filings introduced by the disc mill. Bromoform (specific gravity 2.85) was used to separate dense grains from the more abundant grains of quartz and feldspar. About 30 g of sample was placed in bromoform and stirred to aid in separation. Once settled, dense separates were flushed out of a separatory funnel. Separates were mounted in UV-curing epoxy and were polished with 1 μm α-alumina on a Struers Polisher to prepare for examination with a Tescan Vega TS5136 scanning electron microscope (SEM). Mounted K-feldspar and perthite thick sections were also examined by the SEM for textural observations and for obtaining EDS measurements on microperthite.

About 20 mg of each sample was dissolved for isotopic analysis. Each powder was placed in a Teflon insert with 2 mL of 13 M HNO_3 and 50 μL to 100 μL of 29 M HF, dependent on sample mass. The Teflon inserts were placed in steel jackets. Samples were removed after 48 hours at 180°C, and evaporated on a hot plate at 170°C for 2 hours. The residue was then dissolved in 550 μL of 3.5 M HNO_3.

Samples were then centrifuged and put through Sr-specific ion exchange columns using Eichrom Sr Spec resin (Eichrom Technologies). Each column was pre-rinsed with water and HNO_3. 500μL of sample solution was placed into each column. Once the samples completely drained, several cycles of 3.5 M HNO_3 were rinsed through the elution to remove all cations but

Sr. Distilled water flushed the column to evacuate remaining Sr into a collection beaker. About 30 μL (one drop) of H_3PO_4 was added to the eluted material to minimize evaporation. The solution was then evaporated until a small bead (~1 μL) remained.

Each Sr residue was mixed with 2 μL of 2M HCL and 2 μL of $TaCl_5$ solution, to aid Sr ionization. 2 μL load solution was loaded onto a rhenium filament. All analyses were conducted on a VG Sector 54 thermal ionization mass spectrometer, measuring $^{87}Sr/^{86}Sr$, $^{84}Sr/^{86}Sr$, and $^{86}Sr/^{88}Sr$ ratios. Tripoli software was used for data reduction. A Rigaku Supermini X-ray fluorescence spectrometer was used to measure concentrations of Rb and Sr. XRF discs were prepared by mixing 10.000 g of finely crushed whole rock with 4.000 g of a mixture of 5% elvacite binder in acetone. After the material was mixed, it was allowed to sit overnight. After re-crushing in a ceramic mortar, the material was pressed into an aluminum cap at 50,000 psi. The XRF was calibrated against various USGS standards for Rb and Sr. Rb and Sr intensities were normalized to the intensity of the Pd Compton peak to correct for the mass absorption coefficient of each sample.

DATA

Rb-Sr isotopic ratios were measured for 11 samples from across the TIS, including eight pegmatite, one metasedimentary, and two granitoid samples. Sr isotopic ratios, Rb and Sr concentrations, and unit-wide age ranges from Coleman and Glazner (1997), Coleman et al. (2004), Matzel et al. (2005, 2006), and Memeti et al. (2011) were used to calculate initial $^{87}Sr/^{86}Sr$. These initial ratios were then compared with those of granitoids and wall rocks from Kistler et al. (1986), Bateman et al. (1988), Gray et al. (2008), Mills et al. (2009), and Gross (2015).

Initial $^{87}Sr/^{86}Sr$ of Pegmatite

Previous U-Pb zircon geochronological data were used to estimate the pegmatites' crystallization ages. Measured Sr isotopic ratios, Sr and Rb concentrations, and literature age ranges for corresponding units were applied to the ^{87}Rb decay equation to provide ranges of initial $^{87}Sr/^{86}Sr$. Ages for corresponding units and initial $^{87}Sr/^{86}Sr$ are all listed in Table 1. Literature ages consisted of the whole range of U-Pb zircon ages for particular units where pegmatites were located (Coleman and Glazner, 1997; Coleman et al., 2004; Matzel et al., 2005, 2006; Memeti, et al., 2011). The entire TIS was assembled from about 95 Ma to 85 Ma (Coleman et al., 2004), so this represents a maximum range for pegmatite crystallization ages. Age correction yielded two ranges of initial $^{87}Sr/^{86}Sr$ for each sample: one for a unit-wide age span and a larger uncertainty for the whole-suite age span. Age-related uncertainty is far greater than the analytical uncertainty of $^{87}Sr/^{86}Sr$ calculations. The variation in initial $^{87}Sr/^{86}Sr$ is a function of the age range and the Rb/Sr ratio (Fig. 4). Initial $^{87}Sr/^{86}Sr$ ranges are represented by the distance between y-intercepts of the isochrons shown.

Initial $^{87}Sr/^{86}Sr$ is spatially variable across the TIS. The May Lake and Saddlebag Lake areas have pegmatites with higher initial $^{87}Sr/^{86}Sr$ than those located in Khdp (Fig. 5). Average initial $^{87}Sr/^{86}Sr$ of pegmatite near May Lake is 0.7090 and near Saddlebag Lake is 0.7073. Initial $^{87}Sr/^{86}Sr$ for pegmatites on the interior portions of the suite is 0.7066. Ranges of $^{87}Sr/^{86}Sr$ for granitoids in corresponding units are shown as green bands in Figure 5. Nearly all of the pegmatites have elevated $^{87}Sr/^{86}Sr$ compared to the plutonic rocks of the TIS.

Table 1: Rb-Sr Isotopic Data

Names	Type	Rb ppm	Sr ppm	$^{87}Rb/^{86}Sr$	$^{87}Sr/^{86}Sr$	$^{87}Sr/^{86}Sr_i$	Age est. (Ma)*
MLM1	Metasedimentary	25	155	0.43716	0.726575	0.72599	93.3 ± 0.9
MLP1	Pegmatite	427	51	23.02729	0.739894	0.70930	93.3 ± 0.9
MLP2	Pegmatite	378	72	14.40508	0.727831	0.70869	93.3 ± 0.9
NP1	Pegmatite	170	244	1.89920	0.708768	0.70637	87.2 ± 1.1
NPGD	Granodiorite	149	539	0.75424	0.707347	0.70640	87.2 ± 1.1
OPP1	Pegmatite	223	46	13.13755	0.724164	0.70699	90.5 ± 1.5
QPGD	Granodiorite	143	499	0.78087	0.707167	0.70615	90.5 ± 1.5
QPP1	Pegmatite	226	109	5.68362	0.713776	0.70635	90.5 ± 1.5
SLP1	Pegmatite	276	97	7.77577	0.717811	0.70800	87.2 ± 1.1
SLP2	Pegmatite	266	58	12.47706	0.722009	0.70627	87.2 ± 1.1
SLP3	Pegmatite	289	94	8.39798	0.717634	0.70704	87.2 ± 1.1

*****Ages are from geochronological data from Coleman et al. (2004), Coleman and Glazner (1997), Matzel et al. (2005, 2006), and Memeti et al. (2011). Margins of uncertainty represent extreme ranges from the sources listed above.

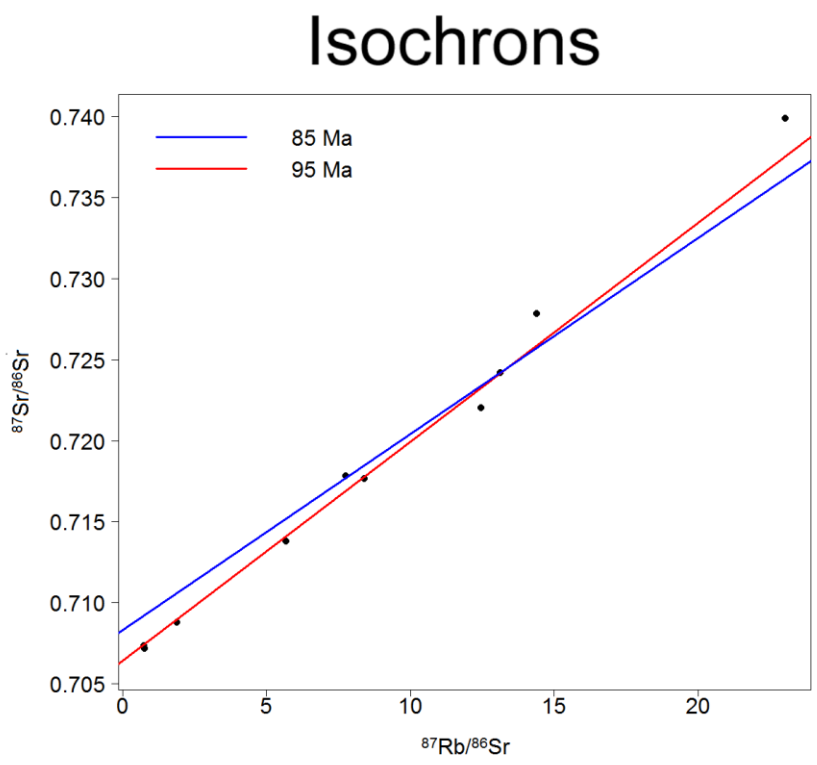

Figure 4: Intercepts of age correction lines show the initial Sr ratios of OPP1 given the maximum age range of 90 ± 5 Ma (Coleman et al., 2004). The initial $^{87}Sr/^{86}Sr$ experiences a relatively small change even at this maximum age range.

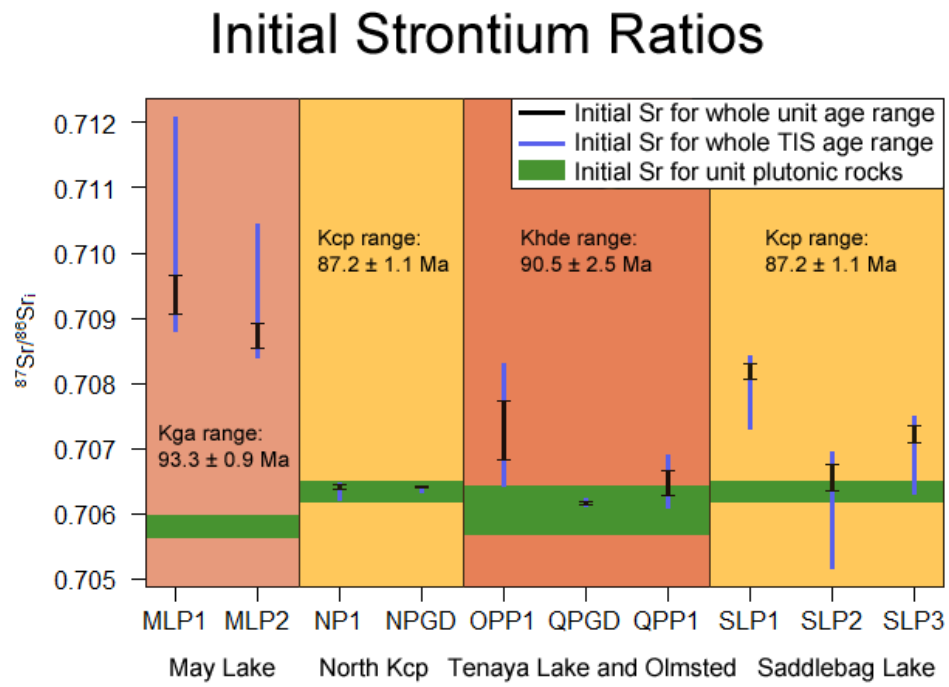

Figure 5: Ranges of $^{87}Sr/^{86}Sr$ of igneous samples from across the Tuolumne Intrusive Suite. Blue lines show maximum extents of possible $^{87}Sr/^{86}Sr_i$ if the values are corrected to the age range of the entire TIS. Black lines represent $^{87}Sr/^{86}Sr_i$ corrected to the age ranges of units, with data from Coleman et al. (2004). Green bands represent $^{87}Sr/^{86}Sr_i$ for granitoids in the corresponding units.

Electron Microscopy

SEM imagery of feldspars form May Lake and Saddlebag Lake was used for both textural observations and semi-quantitative analyses. Perthite lamellae are among the most ubiquitous textural features. Cracks occur locally on-axis with the perthite lamellae. Parallel linear features that are oblique to the general orientation of perthite extend through the feldspar from MLP1. Narrow, tightly packed perthite lamellae truncate asymptotically against these features (Fig. 6E). Perthite lamellae are also present but less continuous throughout SLP2. Perthite lamellae compositions are around $An_4Or_1Ab_{95}$, and the K-feldspar is around $An_0Or_{90}Ab_{10}$ (Fig. 7). Not all albite appears to have formed by exsolution; granular, zoned albite in MLP1 contains graphic quartz and more abrupt margins with surrounding K-feldspar (Fig 6B).

Small speckled features are ubiquitous in both feldspar (Fig. 6A) and quartz (Fig. 6C), and in both localities (Fig. 6D). These speckled features appear in and out of focus in Figure 6A despite an even surface. These are likely not polishing artifacts due to their nonlinear shapes. The out-of-focus patches may represent features below the polished surface, such as fluid inclusions. K-feldspar and albite domains appear as patches in samples from both localities. This change in brightness signifies a slight difference in the mean atomic number and may reflect changes in the K/Na ratio or Ba content (Johnson and Glazner, 2010). Major element compositions did not change appreciably when X-ray point analyses were taken across these patches.

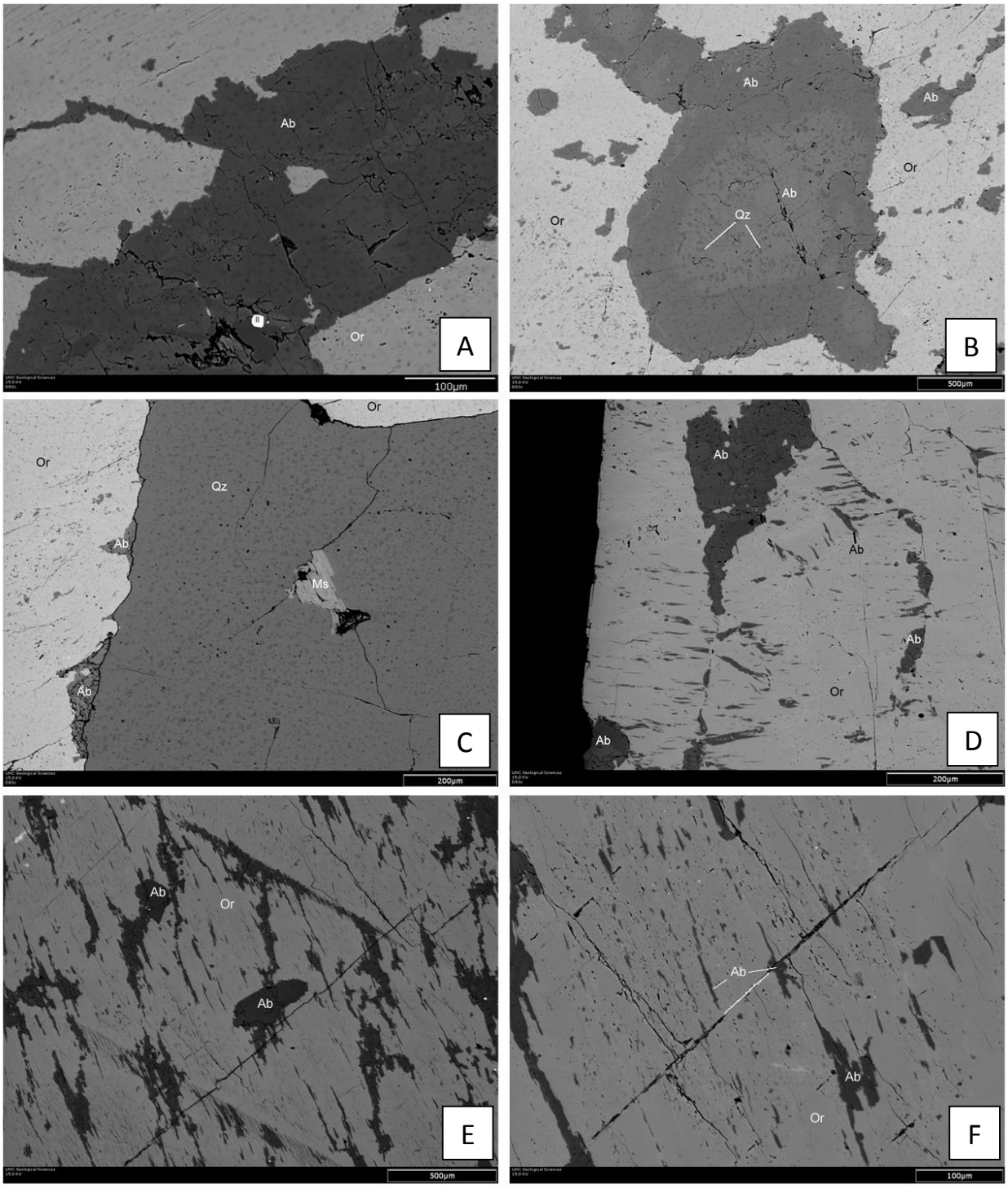

Figure 6: A, B, and C are pegmatites from May Lake, and D is a pegmatite from near Saddlebag Lake. E and F show polished sections of MLP1. A) Perthite lamellae (Ab) in a K-feldspar matrix (Or). Bright grains are Fe-Ti oxides (Il). B) Zoned albite containing graphic quartz. C) Quartz containing muscovite (ms) adjacent to albite and K-feldspar. D) K-feldspar with perthite oriented perpendicular to common axes. E) Parallel perthite-free bands in pegmatitic K-feldspar from near May Lake. F) Perthite from May Lake with indistinct margins between K-feldspar and albite domains.

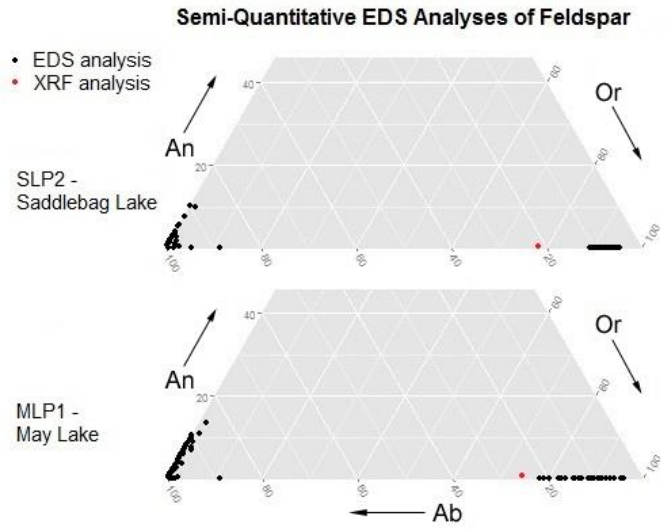

Figure 7: Semi-Quantitative X-ray spot analyses for feldspars from SLP2 and MLP1. Whole feldspar compositions were determined by XRF. Major element oxide composition was converted to feldspar components by methods described in Deer et al., 2013

DISCUSSION

Conditions

Major element oxide compositions of perthite domains were compared to assess the extent of exsolution in pegmatitic K-feldspar. MgO, TiO_2, and Fe_2O_3 comprise less than 0.3% of K-feldspars analyzed by XRF, suggesting the crystals were relatively free of inclusions. The whole-feldspar analyses of May Lake and Saddlebag Lake K-feldspars were closer to the orthoclase end, at about Or_{75}. This composition is expected, given proportions of perthite lamellae and K-feldspar observed in BSE images.

Compositions of K-feldspar and perthitic albite, plot on opposite ends of the feldspar ternary diagram (Fig. 7). The bulk compositions were roughly Or_{75}, the albite domains were about Ab_{95}, and the K-feldspar was about Or_{90} (Fig. 7). These bimodal feldspar compositions indicate that pegmatites continued to develop at temperatures as low as 400°C (Glazner and Johnson, 2013). The implied cooling required for these feldspar compositions is consistent with the late stage nature of pegmatites (Jahns and Burnham, 1969; Glazner and Johnson, 2013). The

peristerite solvus may also have been involved in generating compositional variability in feldspars along the albite end of the ternary diagram (Johnson and Glazner, 2010).

Electron microscopy of K-feldspars, the most abundant phase in sampled pegmatites, supports low-temperature, late stage pegmatite development. The presence of possible fluid inclusions in quartz and K-feldspar (Fig. 6A) may signify high water contents required to crystallize pegmatite (Jahns and Burnham, 1969; Nabelek et al., 2010, Davison and Thomas, 2012). High water contents in pegmatite parental magmas reduce viscosity, enabling circulation through surrounding rock.

Spatial Variation in $^{87}Sr/^{86}Sr_i$

Initial $^{87}Sr/^{86}Sr$ calculated from whole rock Rb-Sr TIMS analyses were compared with surrounding granitoids and nearby metasedimentary wall rocks by projecting initial $^{87}Sr/^{86}Sr$ for pegmatites, granitoids (Kistler et al., 1986; Bateman et al., 1988; Gray et al., 2008), and wall rocks (Mills et al., 2009; Gross, 2015) onto transects A – A' and B – B' (Figs. 1, 8A, and 8B). Due to the limited spatial extent of wall rocks from near May Lake in Mills et al. (2009), I assumed that they are all located at the same point along the A – A' transect. Plotting initial $^{87}Sr/^{86}Sr$ and $^{87}Sr/^{86}Sr_{90}$ versus distance to the nearest contact provides spatial context for isotopic variation (Fig. 9).

Generally, pegmatites near the margins of the TIS have initial $^{87}Sr/^{86}Sr$ between granitoids and adjacent wall rocks (figure 8A and 9). These pegmatites are significantly more radiogenic than the granitoids which they intrude (Fig. 5). Of all pegmatite samples along the margins, only one has an uncertainty in $^{87}Sr/^{86}Sr_i$ which overlaps the literature granitoid values.

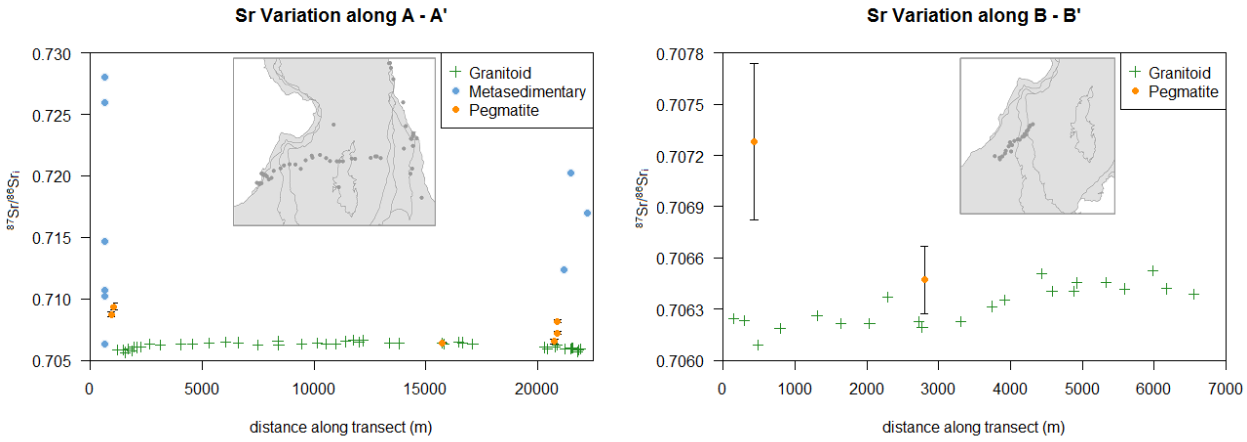

Figure 8: $^{87}Sr/^{86}Sr_i$ projected onto corresponding transects (Fig. 1). Certain points from Mills et al. (2009) have initial Sr greater than 0.730 and plot above the graph extent for 8A.

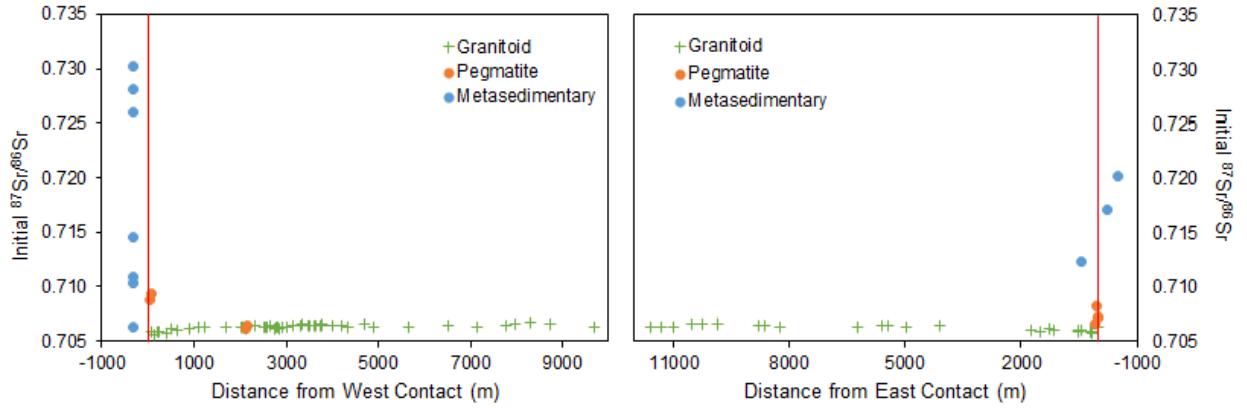

Figure 9: Variation in $^{87}Sr/^{86}Sr_i$ with respect to distance from contact. Some points from Mills et al. (2009) are too high to fit in the map window. Points in each window above do not overlap, and the contact is 0 on the horizontal axis. Points from Mills et al. (2009) are excluded from transect A – A'.

Spatial variation is also apparent when comparing initial $^{87}Sr/^{86}Sr$ with distance from the nearest contact. If interaction between wall rocks and granitoids contributed to pegmatite compositions, initial $^{87}Sr/^{86}Sr$ of pegmatites along the exterior of the TIS should be greater than those on the interior. Although comparing the isotopic data to contact distance shows similar patterns to transect projections (Figs. 8A, 8B, and 9) this absolute spatial comparison more accurately depicts the distance from pegmatites to the contacts.

Models which invoke simple fractional crystallization (Jahns and Burnham, 1969; Roda-Robles, 2012) cannot solely account for differences in isotopic compositions between pegmatites and plutonic rocks of the TIS. Some external fluid or magmatic source must have contributed to the system prior to pegmatites' rapid crystallization. The proximity between more radiogenic pegmatites and wall rock, along with the intermediate pegmatite $^{87}Sr/^{86}Sr_i$ suggest that mass transfer between metasedimentary wall rock and surrounding granitoids contributed to the whole-rock isotopic variation.

Mechanisms

Hypothetical mixing curves were calculated between several metasedimentary and granitoid samples to determine whether exposed compositions can account for pegmatite compositions. The bulk mixing of two magmas should produce compositions along a hyperbola between endmembers, when comparing initial $^{87}Sr/^{86}Sr$ and Sr concentration. Compositions of pegmatites are distinct from most of the calculated mixing curves between the wall rocks and granitoid samples (Fig. 10). Curves which overlap the pegmatite data imply that pegmatites are composed of about 90% wall rock. This ratio of wall rock to granitoid is unlikely, given pegmatites' low-temperature development (Jahns and Burnham, 1969). If chemical interaction via mixing occurred between intruding magma and wall rocks, at least one of the two endmembers had a composition distinct from units currently exposed.

A more realistic endmember is depicted by the red curve in Figure 10. This curve represents mixing between one of the wall rocks with lower $^{87}Sr/^{86}Sr_{90}$ and a fluid derived from a granitic magma. Fluids exsolved from crystallizing magma would likely have lower Sr concentrations but identical initial $^{87}Sr/^{86}Sr$ as the granitic magma from which the fluid was

derived. This mixing curve passes through the pegmatite field (Fig. 10) and may represent a possible set of mixing compositions.

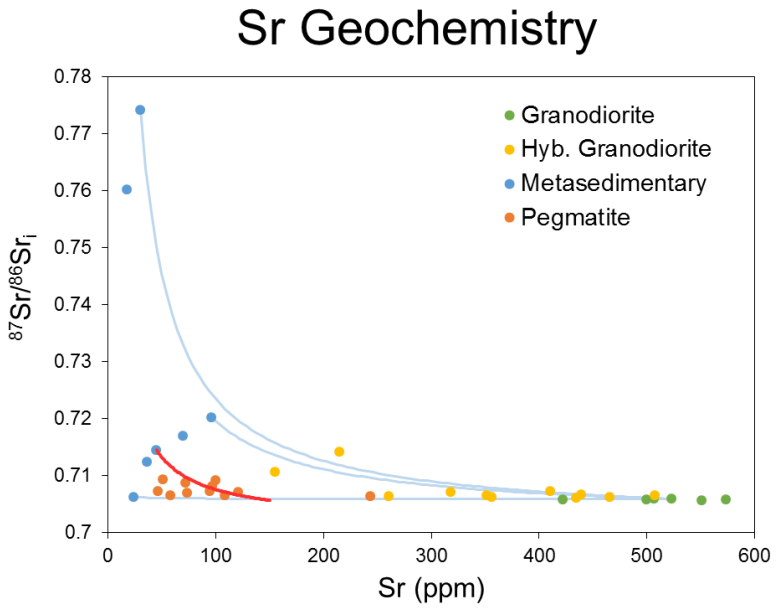

Figure 10: Comparison of initial $^{87}Sr/^{86}Sr$ with Sr concentration for materials near May Lake. Granitoids and wall rocks are from near May Lake, and pegmatite points are from across the Tuolumne Intrusive Suite. Blue curves are calculated mixing curves between several measured compositions. The red mixing curve is calculated between a less radiogenic wall rock sample and a hypothetical, Sr-depleted granitoid derived fluid.

The spread of wall rock isotopic data limits estimates of wall rock-related endmembers. A partial melt depleted in Sr may be a more realistic wall rock endmember. However, mixing of partial melts and hydrothermal derivatives may account for pegmatite isotopic compositions in the TIS. The inability for samples to fall on a mixing curve suggests that more complex processes were involved, perhaps combining partial melting of wall rock and fractional crystallization of magmatic pulses. Additional, unobserved endmembers cannot be ruled out. Mass exchange by circulation of fluids through the surrounding wall rock is consistent with the variation of initial $^{87}Sr/^{86}Sr$ between pegmatites, wall rocks, and plutonic rocks throughout the TIS.

CONCLUSIONS

Pegmatites' elevated initial $^{87}Sr/^{86}Sr$ and low Sr concentration, compared to plutonic rocks, suggest that pegmatites formed by the interaction of hydrothermal fluids with more

radiogenic wall rock on the margins of the TIS. Hydrothermal fluids circulated through surrounding wall rocks, and acquired a wall rock isotopic signature. This intermediate initial $^{87}Sr/^{86}Sr$ was subsequently preserved in pegmatites. Neither fractional crystallization of granitic magma, nor bulk mixing of exposed compositions can exclusively account for the intermediate initial $^{87}Sr/^{86}Sr$ of pegmatites along the margins and interior of the TIS. These isotopic data do not preclude the possibility that external hydrothermal fluids entered the system and contributed to pegmatite isotopic compositions.

Obtaining isotopic data from pegmatite dikes in Kjp and from additional locations along TIS-wall rock margins would further test the hypothesis that pegmatites record fluid-wall rock interaction. If pegmatites from the interior of the TIS have initial $^{87}Sr/^{86}Sr$ within the range of Kjp initial $^{87}Sr/^{86}Sr$, this would support the aforementioned hypothesis. Elevated initial $^{87}Sr/^{86}Sr$ for pegmatites on the TIS interior would suggest that another mechanism or crustal fluid contributed to isotopic variation.

ACKNOLEDGEMENTS

Many thanks go to Dr. Allen Glazner, Dr. Drew Coleman, Dr. Ryan Mills, and Jonathan Munnikhuis for all of their invaluable guidance on this project. I thank Dr. Coleman for giving me the opportunity to obtain isotopic data with the VG Sector 54 TIMS in his lab at UNC-Chapel Hill. I would also like to thank Jonathan Munnikhuis for inviting me to serve as his field assistant and Dr. Coleman for lending his experience in the field. I thank Sean Gaynor, Connor Lawrence, and Ryan Frazer for their willingness to train me on various geochemical preparation techniques. Finally, Dr. Glazner, Jonathan Munnikhuis, and Tyler Wickland provided crucial feedback on the writing and presentation of this work. This project was supported by the Charles

and Elaine Mims Fellowship, administered by the Department of Geological Sciences at the University of North Carolina at Chapel Hill.

REFERENCES

Ballouard, C., Boulvais, P., Poujol, M., Gapais, D., Yamato, P., Tartèse, R., Cuney, M., 2015, Tectonic record, magmatic history and hydrothermal alteration in the Hercynian Guèrande leucogranite, Armorican Massif, France: Lithos, v. 220-223, p. 1-22.

Bateman, P. C., and Chappell, B. W., 1979, Crystallization, fractionation, and solidification of the Tuolumne Intrusive Series, Yosemite National Park, California: Geological Society of America Bulletin, v. 90, no. 5, p. 465-482.

Bateman, P. C., Chappell, B. W., Kistler, R. W., Peck, D. L., Busacca, A. J., 1988, Tuolumne Meadows Quadrangle, California; analytic data: U.S. Geological Survey Bulletin (B 1819), 43 p.

Blasi, A., De Pol Blasi, C., Zanazzi, P. F., 1987, A re-examination of the Pellotsalo microcline: mineralogical implications and genetic considerations: The Canadian Mineralogist, v. 25, p. 527-537.

Brook, C. A., 1977, Stratigraphy and structure of the Saddlebag Lake roof pendant, Sierra Nevada, California: Geological Society of America Bulletin, v. 88, p. 321-334.

Coleman, D. S., and Glazner, A. F., 1997, The Sierra Crest Magmatic Event: rapid formation of juvenile crust during the late Cretaceous in California: International Geology Review, v. 39, no. 9, p. 768-787, doi: 10.1080/00206819709465302.

Coleman, D. S., Gray, W., Glazner, A. F., 2004, Rethinking the emplacement and evolution of zoned plutons: Geochronologic evidence for incremental assembly of the Tuolumne Intrusive Suite, California: Geology, v. 32, no. 5, p. 433-436, doi: 10.1130/G20220.1.

Deer, W.A., Howie, R.A., Zussman, J., 2013, An introduction to the rock-forming minerals: London, United Kingdom, the Mineralogical Society, Ed. 3, 498 p.

Eichrom Technologies, 2016, Eichrom: Sr Resin: http://www.eichrom.com/eichrom/products/info/sr_resin.aspx

Glazner, A. F., and Johnson, B. R., 2013, Late crystallization of K-feldspar and the paradox of megacrystic granites: Contributions to Mineralogy and petrology, v. 166, p. 777-799.

Gray, W., Glazner, A. F., Coleman, D. S., Bartley, J. M., 2008, Long-term geochemical variability of the late Cretaceous Tuolumne Intrusive Suite, central Sierra Nevada California: Geological Society Special Publications, v. 304, p. 183-201.

Gross, A., 2015. Rare earth element and trace element analysis of country rock of the Sierra Nevada Batholith [Senior Thesis]: Chapel Hill, University of North Carolina, 14 p.

Interdisciplinary Earth Data Alliance, 2016, System for Earth Sample Registration: http://www.geosamples.org/

Jahns, R. H., and Burnham, C. W., 1969, Experimental studies of pegmatite genesis: I. A model for the derivation and crystallization of granitic pegmatites: Economic Geology, v. 64, no. 9, p. 843-864.

Johnson, B. R., and Glazner, A. F., 2010, Formation of K-feldspar megacrysts in granodioritic plutons by thermal cycling and late-stage textural coarsening: Contributions to Mineralogy and Petrology, v. 159, p. 599-619.

Lahren, M. M., and Schweickert, R. A., 1990, Evidence of uppermost Proterozoic to lower Cambrian miogeoclinal rocks and the Mojave-Snow Lake fault: Snow Lake Pendant, central Sierra Nevada, California: Tectonics, v. 9, no. 6, p. 1585-1608.

Kistler, R. W., Chappell, B. W., Peck, D. L., Bateman, P. C., 1986, Isotopic variation in the Tuolumne Intrusive Suite, central Sierra Nevada, California: Contributions to Mineralogy and Petrology, v. 94, p. 205-220.

Kontak, D. J., Dostal, J., Kyser, T. K., Archibald, D. A., 2002, A petrological, geochemical, isotopic and fluid-inclusion study of 370 Ma pegmatite-aplite sheets, Peggy's Cove, Nova Scotia, Canada: The Canadian Mineralogist, v. 40, no. 5, p. 1249-1286.

Matzel, J., Mundil, R., Paterson, S., Renne, P., and Nomade, S., 2005, Evaluating pluton growth models using high resolution geochronology: Tuolumne intrusive suite, Sierra Nevada, CA: Geological Society of America Abstracts with Programs, v. 37, no. 7, p. 131

Matzel, J., Miller, J.S., Mundil, R., and Paterson, S.R., 2006, Zircon saturation and the growth of the Cathedral Peak pluton, CA: Geochimica et Cosmochimica Acta, v. 70, no. 18, p. A403, doi: 10.1016/j.gca.2006.06.813.

Memeti, V., Patterson, S., Matzel, J., Mundil, R., and Okaya, D., 2010, Magmatic lobes as snapshots" of magma chamber growth and evolution in large, composite batholiths: An example from the Tuolumne intrusion, Sierra Nevada, California: Geological Society of America Bulletin, v. 122, p. 1912-1931.

Mills, R. D., Glazner, A. F., Coleman, D. S., 2009, Scale of pluton/wall rock interaction near May Lake, Yosemite National Park, CA, USA: Contributions to Mineralogy and Petrology, v. 158, p. 263-281, doi: 10.1007/s00410-009-0381-x.

Nabelek, P. I., Wittington, A. G., Sirbescu, M. C., 2010, The role of H_2O in rapid emplacement and crystallization of granite pegmatites: resolving the paradox of large crystals in highly undercooled melts: Contributions to Mineralogy and Petrology, v. 160, p. 313-325, doi: 10.1007/s00410-009-0479-1.

O'Meara, S., 2006, Digital geologic map of Yosemite National Park and vicinity, California (NPS, GRD, GRE, YOSE): NPS Geologic Resources Inventory Program. Lakewood, CO.

Phillips, M. W., Ribbe, P. H., 1973, The structures of monoclinic potassium-rich feldspars: The American Mineralogist, v. 58, p. 263-270.

Roda-Robles, E., Pesquera, A., Gil-Crespo, P., Torres-Ruiz, J., 2012, From granite to highly evolved pegmatite: a case study of the Pinilla de Fermoselle granite-pegmatite system (Zamora, Spain): Lithos, v. 153, p. 192-207.

Rose, R. L., 1957, Andalusite- and corundum-bearing pegmatites in Yosemite National Park, California: The American Mineralogist, v. 42, p. 635-647.

Simmons, W. B., and Webber, K. L., 2008, Pegmatite genesis: state of the art: European Journal of Mineralogy, v. 20, p. 421-438,

Thomas, R., and Davidson, P., 2012, Water in granite and pegmatite-forming melts: Ore Geology Reviews, v. 46, p. 32-46.

Veksler, I. V., Thomas, R., Schmidt, C., 2002, Experimental evidence of three coexisting immiscible fluids in synthetic granitic pegmatite: American Mineralogist, v. 87, p. 775-779.